

NUMERICAL INVESTIGATION OF BUOYANCY DRIVEN LAMINAR FLOW IN A DIFFERENTIALLY HEATED CAVITY

Tuhami M. Jaballa, Jamal S. Hawisa* and Mohamed T. Rakhiyes**

Department of Mechanical Engineering, Faculty Engineering, University of Tripoli, *

*CNG, & Advisor to NOC Board

**The GEC of Libya Tripoli-Libya

E-mail: t.jaballa@uot.edu.ly

المخلص

أجريت دراسة عددية ثنائية الأبعاد لانتقال الحرارة بالحمل الحر للهواء في تجويف مربع مغلق. يتعرض الجدار العمودي الأيسر إلى تسخين بينما تم تثبيت درجة حرارة الجدار العمودي في الجهة اليمنى عند درجة حرارة منخفضة. وقد اعتبرت الأسطح العليا والسفلى معزولة. تضمنت الدراسة الحل العددي لمعادلات نافير-ستوك ومعادلة الطاقة باستخدام طريقة الحجم المحدد. استخدمت خوارزمية (SIMPLE) لحل معادلات الكتلة وكمية الحركة والطاقة، بلغة (FORTRAN 90) لحساب السرعة ودالة الانسياب ودرجات الحرارة للمجال الحسابي.

تم اعتبار أن عدد براندل ثابت ويساوي 0.71، بينما يتغير عدد رايلي من 10^3 إلى 10^8 . وجد أن انتقال الحرارة يكون بالتوصيل فقط لقيم رايلي عند 10^3 وأن انتقال الحرارة يبدأ بالتحول إلى الحمل مع ازدياد عدد رايلي. ومن أجل التحقق من مصداقية الحل العددي، تم مقارنة النتائج المتحصل عليها مع بحوث سابقة لكل من عدد نسلت المتوسط والقيم القصوى والدنيا لعدد نسلت المحلي على طول الجدار الساخن وكذلك أقصى سرعة وأدنى سرعة ومكان حدوثها لجميع أرقام عدد رايلي المذكورة. بينت النتائج العددية توافقاً جيداً مع منشورات سابقة. وكانت النتائج لعدد نسلت المحلي الأقصى وعدد نسلت المتوسط ضمن 0.22% و 0.7% على التوالي. كما قورنت نتائج خطوط الجريان وخطوط درجات الحرارة وأظهرت توافقاً جيداً.

ABSTRACT

Two-dimensional natural convection heat transfer in a differentially heated square cavity was examined numerically. The left sidewall of the cavity was heated, while the right side was kept at constant lower temperature. The top and bottom walls were adiabatic. The theoretical study involved the numerical solution of the Navier-Stokes and energy equations by using finite volume method. A computational code based on the SIMPLE algorithm was used for the solution of the system of mass, momentum, and energy transfer governing equations. The prepared numerical solution was capable of calculating the velocity, stream function and the temperature fields of the computational domain. A computer program in (FORTRAN 90) was used to carry out the numerical solution.

The problem has been analyzed and made dimensionless. The non-dimensional governing equations were solved using finite volume method. The enclosure was assumed to be filled with air of a Prandtl number of 0.71. The problem was examined for different values of Rayleigh numbers in the range from 10^3 to 10^8 . It was found that the heat transfer was dominated by conduction for small Ra of 10^3 , and began to be dominated by convection with increasing Ra. In order to validate the numerical model; average Nusselt number, local Nusselt number along the hot wall, its maximum and minimum values and

the locations where they occur, the maximum and minimum velocity values and their corresponding locations for all values of Ra are compared with previous works. The model results were found to be in an excellent agreement with previous literature results which validate the present computational model. The model predictions of the maximum local Nusselt number and the average Nusselt number were within 0.22% and 0.7% respectively. The results of streamlines and isotherms are compared with data found in literature and an acceptable agreement was found.

KEYWORDS: Natural Convection; Finite Volume Method; Nusselt Number; Square Enclosure; Rayleigh Number; differentially heated cavity.

INTRODUCTION

Buoyancy-driven convection in a square cavity with differentially heated isothermal walls is a prototype of many industrial applications such as thermal insulation, cooling of electronic devices, solar energy instruments, nuclear reactors, heat-recovery systems, room ventilation, etc. Buoyancy driven flows are complex because of essential coupling between the transport properties of flow and thermal fields.

This research presents a computational method of study to obtain the solutions of the buoyancy-driven laminar flow heat transfer in a two-dimensional natural convection of an air-filled cavity. There are numerous commercial CFD codes available on the market. They are user-friendly robust and convenient. It's easy to perform a CFD simulation by using a commercial CFD code. However, the solver is often operated as a "black box"; the encapsulation of the commercial codes makes them blind to the users. User has no access to the detailed codes and cannot debug the program, which limits its function in the teaching and research activities because researchers always need full control of the codes and want to keep track of the change of every variable.

RESEARCH OBJECTIVE

Analysis of heat transfer within the fluid flow is important since it has many applications in industries such as energy conservation process, energy storage, meteorology and climatology. Numerical simulation plays an important role in these areas because experiments are often costly. The objectives of this research are meant to:

- i. Study the phenomena of natural convection inside a two-dimensional enclosure, which is differentially heated and cooled from the vertical walls.
- ii. Develop Mathematical formulation of the physical problem along with the boundary conditions for a laminar flow in a differentially heated cavity.
- iii. Develop a program based on a finite volume method (FVM) and to validate the applied numerical method for the classical two-dimensional square cavity.
- iv. Investigate and determine the influence of Rayleigh number, Ra , on the velocity and temperature fields inside a two-dimensional square cavity.

LITERATURES SURVEY

Natural convection in rectangular enclosure has been studied for many years. Batchelor (1954) [1] formulated the problem of natural convection in a rectangular cavity where heat transfer characteristics at different Rayleigh numbers were analyzed. Wilkes and Churchill (1966) [2] developed finite difference scheme to study natural convection

in a long horizontal enclosure of rectangular cross section with differentially heated vertical walls. They obtained transient and steady state isotherms and streamlines for wide range of Grashof numbers and different aspect ratios.

De Vahl Davis (1983) [3] presented benchmark numerical solution of natural convection of a square cavity. The study is performed for air with Prandtl number 0.71 and for Rayleigh number changing from 10^3 to 10^6 . The governing equations of motion and heat transfer are solved on several mesh sizes by finite difference method. They tabulated values of average Nusselt number on the vertical boundaries of the cavity. The maximum horizontal and vertical velocities and the maximum absolute value of the stream function at four different Rayleigh numbers for various grid sizes are used by many researchers to check the accuracy of the solution obtained.

Henkes et al (1990) [4,5] carried out two-dimensional calculations in a square cavity which was heated from the vertical walls. The governing equations are solved using several mesh sizes by finite volume method. They used three different discretization schemes; the second-order central differencing, hybrid scheme and first-order upwind scheme. The central difference scheme was found to give the most accurate solutions. The computations covered both laminar and turbulent flows with Rayleigh numbers, ranging up to 10^{14} for air and 10^{15} for water. The last streamline pattern of $Ra > 5 \times 10^6$ contained four asymptotic structures, a vertical boundary layer along the heated wall, a core region, a corner region and a horizontal layer. For increasing Ra , the core became thermally stratified and had horizontal streamlines. For $Ra \rightarrow \infty$, the Navier-Stokes solution along the vertical wall converged to the boundary layer solution.

Le Quéré (1990) [6] has revisited the benchmark results, and he also added benchmark results for two new cases: air at $Ra = 10^7$ and air at $Ra = 10^8$. Le Quere employing pseudo-spectral Chebyshev collocation method in order to solve the Navier-Stokes and energy transport equations written in primitive variables under the Boussinesq approximation. A very important findings are the detachment region at the horizontal adiabatic walls and the large zone of linear thermal stratification of the core. For increasingly higher Rayleigh numbers the flow eventually turns to be unsteady. The onset of the first transition to periodicity and the physical description of the instability mechanism are still in question.

Many researchers, [7, 8, 10, 11] had contributed to the subject, by either proposing a method of solution or by proposing the mathematical numerical model and the suitable grid size generation.

In this study, the effect of Rayleigh number on the flow patterns and the resulting heat transfer is determined. The numerical technique based on the finite volume method (FVM) is applied and a non-uniform grid size is generated. The results at different Nusselt numbers, which represent the rate of heat being transferred, are presented in tables. Stream function and isotherms contours, which demonstrate the fluid flow and thermal distributions inside the cavity, are also given.

MATHEMATICAL MODEL

The mathematical model for the problem under study consists of a set of governing equations equipped with the boundary conditions so that the number of equations are the same as the number of unknowns. Figure (1) shows a vertical section in the square cavity, $L=H$, with the boundary conditions shown on the vertical right and left walls, while the horizontal walls, top and bottom, are considered adiabatic.

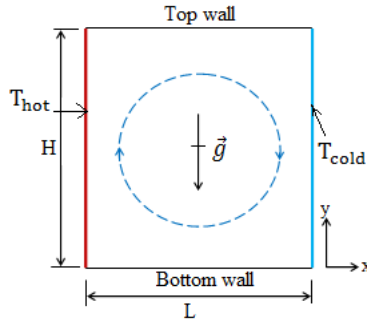


Figure 1: Schematic diagram of the cavity

In building the mathematical model, assumptions of two-dimensional problem without viscous dissipation and with constant properties are made. Gravity effects act in the vertical direction only. Radiation heat exchange was assumed negligible. The governing equations are:

Continuity equation:

$$\frac{\partial(\rho u)}{\partial x} + \frac{\partial \rho v}{\partial y} = 0 \quad (1)$$

X-momentum equation:

$$\frac{\partial}{\partial x}(\rho u u) + \frac{\partial}{\partial y}(\rho v u) = -\frac{\partial p}{\partial x} + \frac{\partial}{\partial x}(\mu \frac{\partial u}{\partial x}) + \frac{\partial}{\partial y}(\mu \frac{\partial u}{\partial y}) + S_{mx} \quad (2)$$

Where,

$$S_{mx} = \left[\frac{\partial}{\partial x}(\mu \frac{\partial u}{\partial x}) + \frac{\partial}{\partial y}(\mu \frac{\partial v}{\partial y}) \right] + \frac{\partial}{\partial x} \left[-\frac{2}{3} \mu \left(\frac{\partial u}{\partial x} + \frac{\partial v}{\partial y} \right) \right] + \rho g_x$$

Y-momentum equation:

$$\frac{\partial}{\partial x}(\rho u v) + \frac{\partial}{\partial y}(\rho v v) = -\frac{\partial p}{\partial y} + \frac{\partial}{\partial x}(\mu \frac{\partial v}{\partial x}) + \frac{\partial}{\partial y}(\mu \frac{\partial v}{\partial y}) + S_{my} \quad (3)$$

Where,

$$S_{my} = \left[\frac{\partial}{\partial x}(\mu \frac{\partial u}{\partial x}) + \frac{\partial}{\partial y}(\mu \frac{\partial v}{\partial y}) \right] + \frac{\partial}{\partial y} \left[-\frac{2}{3} \mu \left(\frac{\partial u}{\partial x} + \frac{\partial v}{\partial y} \right) \right] + \rho g_y$$

Energy equation:

$$\frac{\partial}{\partial x_i}(\rho c u_i T) = \frac{\partial}{\partial x_i} \left(k \frac{\partial T}{\partial x_i} \right) \quad (4)$$

Where the subscript i indicates the tow coordinates x and y, and u_i is u when x_i is x and v when x_i is y.

The governing equations are transformed into non- dimension forms using the following non- dimensional variables:

$$X = \frac{x}{H}, \quad Y = \frac{y}{H}, \quad U = \frac{u}{U_{ref}}, \quad V = \frac{v}{U_{ref}}, \quad \theta = \frac{T - T_c}{T_H - T_c}, \quad P = \frac{p}{P_{ref}}, \quad \mu = \frac{\mu}{\mu_{ref}},$$

$$\rho = \frac{\rho}{\rho_{ref}}$$

Where,

$$U_{ref} = \sqrt{g\beta \cdot \Delta T \cdot H}, \text{ and } P_{ref} = \rho_{ref} U_{ref}^2$$

The resulting governing equations are:

Equation of continuity

$$\frac{\partial \rho U}{\partial X} + \frac{\partial \rho V}{\partial Y} = 0 \quad (5)$$

x-Momentum equation

$$\rho U \frac{\partial U}{\partial X} + \rho V \frac{\partial U}{\partial Y} = -\frac{\partial P}{\partial X} + \sqrt{\frac{\text{Pr}}{\text{Ra}}} \left[\frac{\partial}{\partial X} \left(\mu \frac{\partial U}{\partial X} \right) + \frac{\partial}{\partial Y} \left(\mu \frac{\partial U}{\partial Y} \right) + \frac{\partial}{\partial X} \left(\mu \left(\frac{\partial U}{\partial X} + \frac{\partial V}{\partial Y} \right) \right) \right] \quad (6)$$

y-Momentum equation

$$\rho U \frac{\partial V}{\partial X} + \rho V \frac{\partial V}{\partial Y} = -\frac{\partial P}{\partial Y} + \sqrt{\frac{\text{Pr}}{\text{Ra}}} \left[\frac{\partial}{\partial X} \left(\mu \frac{\partial V}{\partial X} \right) + \frac{\partial}{\partial Y} \left(\mu \frac{\partial V}{\partial Y} \right) + \frac{\partial}{\partial X} \left(\mu \left(\frac{\partial U}{\partial X} + \frac{\partial V}{\partial Y} \right) \right) \right] + \rho \theta \quad (7)$$

Thermal energy equation

$$\rho U \frac{\partial \theta}{\partial X} + \rho V \frac{\partial \theta}{\partial Y} = \frac{1}{\sqrt{\text{Ra Pr}}} \frac{\partial}{\partial X} \left[\mu \frac{\partial \theta}{\partial X} \right] + \frac{1}{\sqrt{\text{Ra Pr}}} \frac{\partial}{\partial Y} \left[\mu \frac{\partial \theta}{\partial Y} \right] \quad (8)$$

Boundary Conditions

The boundary conditions of velocity and temperature fields are shown in Figure (1) and are given below:

			U	V	θ	
S1	West Wall	0	0	0	θ_{\max}	at all Y's, X=0
S2	Top Wall	0	0	$\frac{\partial \theta}{\partial Y} = 0$		at all X's, Y=1. (9)
S3	East Wall	0	0	0	θ_{\min}	at all Y's, X=1.
S4	Bottom Wall	0	0	$\frac{\partial \theta}{\partial Y} = 0$		at all X's, Y=0

The equations (5 to 9) represent the complete mathematical model to be numerically solved. The rate of heat transfer is expressed in terms of local Nusselt number, Nu, at the heated surface as follows:

$$Nu = -\frac{\partial \theta}{\partial X} \Big|_{X=0} \quad (10)$$

The average Nusselt number, \overline{Nu} , is defined by:

$$\overline{Nu} = \frac{1}{H} \int_0^1 \left(-\frac{\partial \theta}{\partial X} \right)_{X=0} dY \quad (11)$$

Noting that at $y=0$, $Y=0$ and at $y=H$, $Y=1$

Grid distribution

At low Rayleigh numbers, non-uniform grid spacing is not essential. At higher Rayleigh numbers, one encounters steep velocity and temperature gradients. Fine grid spacing is required close to the wall to resolve these gradients. The use of non-uniform grid spacing allows an economical distribution of grids in the calculation domain. For laminar calculations, a sine function distribution for the x and y directions is used.

$$\frac{xu(i)}{H} = \frac{i}{i_{\max}} - \frac{1}{2\pi} \sin\left(\frac{2\pi \cdot i}{i_{\max}}\right), \quad i = i_{\min}, i_{\max} \quad (14)$$

$$\frac{yv(j)}{H} = \frac{j}{j_{\max}} - \frac{1}{2\pi} \sin\left(\frac{2\pi \cdot j}{j_{\max}}\right), \quad j = j_{\min}, j_{\max} \quad (15)$$

Notice that $i_{\min}=j_{\min}=2$, $i_{\max}=NI-2$, $j_{\max}=NJ-2$

RESULTS AND DISCUSSIONS:

Grid Sensitivity Check

Test for the accuracy of the grid sensitivity is examined for the arrangements of five different non-uniform grid systems with the following number of elements: 1600, 2500, 3600, 4900 and 6400. The results are shown in Table (1). From these comparisons, it is suggested that 6400 non-uniform elements are sufficient to produce accurate results.

Table 1: Comparison of the Results for Various grid dimensions at $Ra = 10^5$ and $Pr = 0.71$.

Elements	Nusselt Number, Nu
1600	4.502
2500	4.509
3600	4.509
4900	4.510
6400	4.519

Code Validation

In Table (2), a comparison is given between the present laminar solution and numerical results found in the literature. The mean Nu along the hot wall, the maximum and minimum values of Nu , the maximum and minimum velocities and their locations are all compared. The present results are found to have an excellent agreement with the benchmark solution of De Vahl Davis [3] for all values of Ra , and they are within 2% with results of Markatos and Fusegi *et al.*

Table 2: Comparison of 2d DHC flow results with the benchmark data of [dVD, Barakos, Fusegi , A.D’Orazio ,Le 91, Puragliesi] for Ra = 10³, 10⁴, 10⁵, 10⁶, 10⁷, 10⁸.

Ra=10 ³		[dVD83]	[Barakos]	[Fusegi]	[A.D’Orazio]	Present
	\overline{Nu}	1.118	1.114	1.105	1.117	1.117
	Nu_{max}	1.505	1.581	1.420	1.501	1.55
	Position (y/H)	0.092	0.099	0.083	0.086	0.104
	Nu_{min}	0.692	0.670	0.764	0.698	0.655
	Position (y/H)	1.000	0.994	1.000	0.953	0.896
	u_{max}	0.136	1.53	0.132	0.136155	0.135946
	Position (y/H)	0.813	0.806	0.833	0.8125	0.813887
	v_{max}	0.138	1.55	0.131	0.13813	0.138676
	Position (x/H)	0.178	0.181	0.200	0.1797	0.167802

Ra=10 ⁴		[dVD83]	[Barakos]	[Fusegi]	[A.D’Orazio]	Present
	\overline{Nu}	2.243	2.245	2.302	2.235	2.243
	Nu_{max}	3.528	3.539	3.652	3.507	3.53
	Position (y/H)	0.143	0.143	0.623	0.148	0.104
	Nu_{min}	0.586	0.583	0.611	0.584	0.546
	Position (y/H)	1.000	0.994	1.000	0.984	0.992
	u_{max}	0.192	0.193	0.201	0.1992118	0.192118
	Position (y/H)	0.823	0.818	0.817	0.8203	0.8322
	v_{max}	0.234	0.234	0.225	0.234755	0.233624
	Position (x/H)	0.119	0.119	0.117	0.1172	0.11867

Ra=10 ⁵		[dVD83]	[Barakos]	[Fusegi]	[A.D’Orazio]	Present
	\overline{Nu}	4.519	4.510	4.646	4.504	4.519
	Nu_{max}	7.717	7.636	7.795	7.658	7.71
	Position (y/H)	0.081	0.085	0.083	0.088	0.0787
	Nu_{min}	0.729	0.773	0.787	0.728	0.712
	Position (y/H)	1.000	0.999	1.000	0.990	0.998
	u_{max}	0.153	0.132	0.147	0.15331	0.135197
	Position (y/H)	0.855	0.859	0.855	0.8529	0.865943
	v_{max}	0.261	0.258	0.247	0.26146	0.256848
Position (x/H)	0.066	0.066	0.065	0.0637	0.067392	

$Ra=10^6$		[dVD83]	[Barakos]	[Fusegi]	[A.D'Orazio]	Present
	\overline{Nu}	8.800	8.806	9.012	8.767	8.79
	Nu_{max}	17.925	17.442	17.670	17.288	17.5
	Position (y/H)	0.0378	0.0368	0.0379	0.0441	0.0396
	Nu_{min}	0.989	1.001	1.257	0.998	1.04
	Position (y/H)	1.000	0.999	1.000	0.990	0.988
	u_{max}	0.079	0.077	0.084	0.07929	0.078337
	Position (y/H)	0.850	0.859	0.856	0.8529	0.865943
	v_{max}	0.262	0.262	0.259	0.2664182	0.262141
Position (x/H)	0.0379	0.039	0.033	0.0392	0.039597	

$Ra=10^7$		[Le91]	[Puragliesi]	Present
	\overline{Nu}	16.523	16.5231	16.44
	Nu_{max}	39.39	39.3947	39.2
	Position (y/H)	0.018	-	0.0156
	Nu_{min}	1.366	-	1.54
	Position (y/H)	1.000	-	0.996
	u_{max}	0.0470	0.0470	0.052859
	Position (y/H)	0.879	0.8793	0.881325
	v_{max}	0.2211	0.2211	0.264308
Position (x/H)	0.021	0.0213	0.020304	

$Ra=10^8$		[Le91]	[Puragliesi]	Present
	\overline{Nu}	30.225	30.10	30.7
	Nu_{max}	87.24	-	84.2
	Position (y/H)	0.008	-	0.00815
	Nu_{min}	1.919	-	2.69
	Position (y/H)	1.000	-	0.998
	u_{max}	0.8714	0.8231	0.2522287
	Position (y/H)	0.928	-	0.942867
	v_{max}	0.2637	0.2646	0.549264
Position (x/H)	0.012	-	0.047876	

Accuracy Enhancement

Table (3) presents the results obtained for $Ra=10^5$. The central, hybrid and power law differencing schemes were used to discretize the convection-diffusion (advection scheme) terms in this case. Comparisons have been made only with the results of De Vahl Davis. From the table, it is clear that the power law scheme is superior to the hybrid scheme in terms of accuracy. Table (3) gives a comparison between the central, hybrid and power law schemes for the finest grid 80x 80 grid 6400 elements in comparison with the benchmark of De Vahl Davis.

Table 3 : Accuracy of the solution for air at $Ra = 10^5$.

Scheme	Grid	$\overline{NuRa}^{-1/4}$	$\frac{V_{MAX}}{\sqrt{g\beta\Delta TH}}$	$\frac{U_{MAX}}{\sqrt[3]{g\beta\Delta Tv}}$
Central	20×20	0.254740618	0.248474	0.141778
	30×30	0.254009574	0.248042	0.140321
	60×60	0.254065808	0.256777	0.136273
	80×80	0.254459447	0.256918	0.134901
Hybrid	20×20	0.250185653	0.247673	0.141708
	30×30	0.252941126	0.249123	0.140452
	60×60	0.254122043	0.2565536	0.136281
	80×80	0.254346979	0.2556864	0.13488
Power law	20×20	0.251422804	0.245821	0.142641
	30×30	0.252435019	0.248378	0.115417
	60×60	0.253559701	0.256557	0.136757
	80×80	0.254122043	0.256848	0.135197
De Vahl Davis	-	0.254122044	0.261	0.153

The maximum error between the benchmark and present solution occurs for the average Nusselt number, and it is as much as 0.13% for the central scheme. All errors are below 0.13% compared to the benchmark of De Vahl Davis (1984). The power law scheme takes smaller time to obtain the results than the central and hybrid schemes. Thus, the power law scheme is default scheme in the CFD code.

Isotherms and Streamlines

The effect of Rayleigh number ($Ra=10^3$ - 10^8) on isotherms and streamlines are shown in Figure (2) and Figure (3). It is seen that the streamline contours exhibit circulation patterns. One single cell circulation inside the square cavity at $Ra =10^3$ is created, and the cell becomes a circulation of an oval shape at $Ra =10^4$. At $Ra =10^5$ three circulation cells are created because of the temperature difference between the walls. One circulation cell covers most of the cavity apart from the top left corner and the bottom right corner regions, in which the fluid is almost stagnant. Within this primary circulation cell, there are two smaller counter rotating circulation cells near the center of the cavity. At $Ra =10^6$, the two cell circulation move towards the walls, giving space for a third vortex to develop.

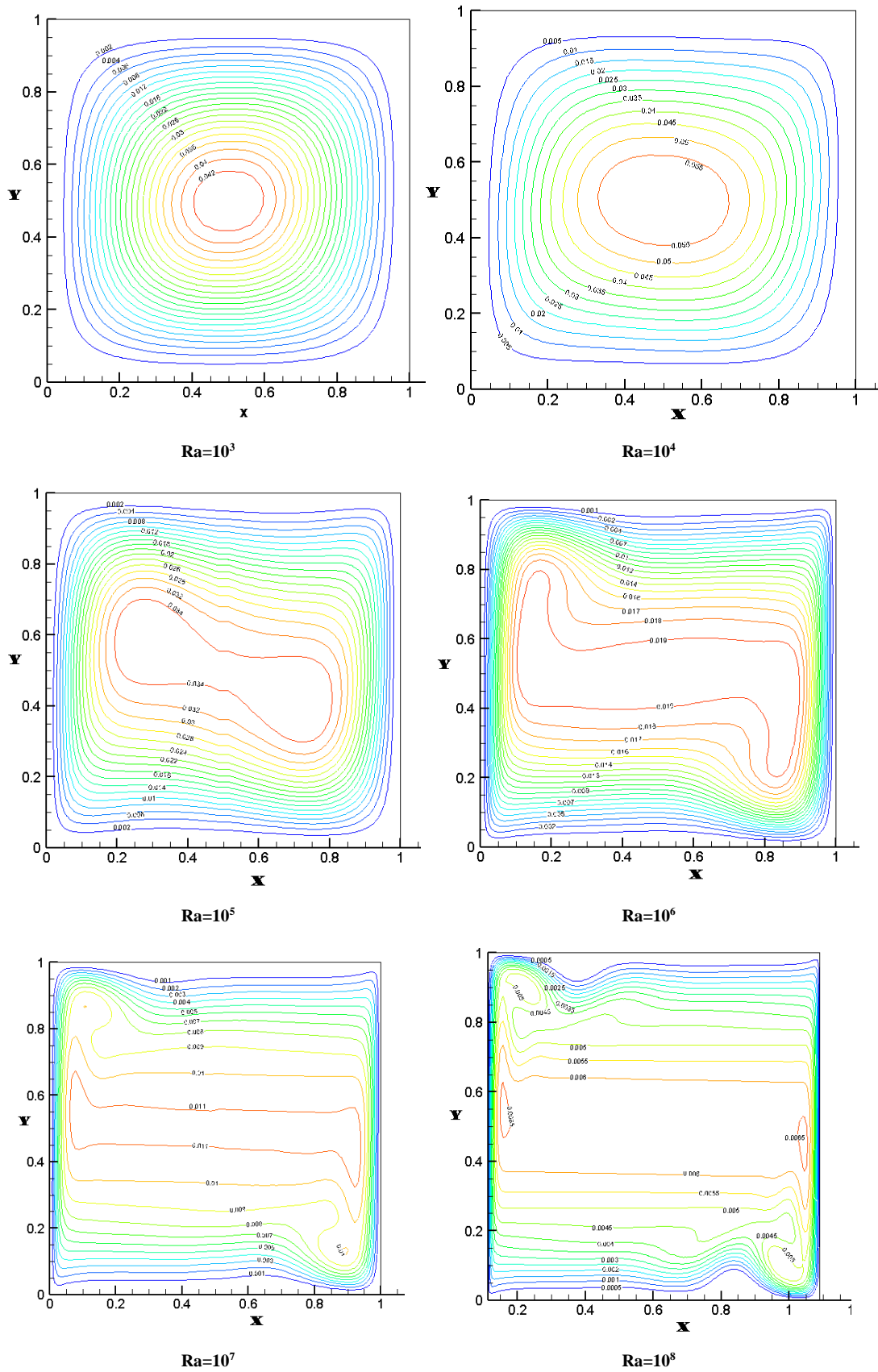


Figure 2: Contour plots of stream-function Ψ for $Ra = 10^3$ - 10^8 .

This third vortex is very weak in comparison with the other two and, the rotation is again clockwise owing to a very small positive temperature gradient at the center of the cavity. The figures also show that the solution is centro-symmetric. At $Ra = 10^7$, the central part of the cavity still has three clockwise cells and two saddle points. However, the upper left and lower right corners of the cavity have developed strong rotating cells or vortices. Similar flow patterns were observed by Henkes (1990) [5].

The shapes of the isotherms, Figure (3), show how the dominant heat transfer mechanism changes as Ra increases. For low Ra -values almost vertical isotherms appear, because heat is transferred by conduction between hot and cold walls. As the isotherms, depart from the vertical position, the heat transfer mechanism changes from conduction to convection. It can be seen that the isotherms at the mid-point between the hot and cold walls of the cavity are horizontal and become vertical only inside the very thin boundary layers.

The temperature contours, θ , reveal that within the top left corner and the bottom right corner heat is transferred almost in conduction mode only, because of almost stagnant fluid and weak convection in those regions. The temperature contours show that the temperature in the core of the square cavity remains almost constant and equal to the average temperature of the hot and the cold walls. The temperature distribution near the top and the bottom walls is slightly modified.

The velocity distribution

It is evident from Figure (4) and Figure (5) that both U and V components are zero at the walls due to no-slip condition, and that they are zero at the center of the cavity, because of the nearly stagnant condition in the center of the vortex formed at the center of the cavity. The U and V distributions are shown to be symmetric relative to the center of the cavity. Since the left wall is heated and the right one is cooled, the fluid is moving upward at the left wall (Positive V at $x/L = 0$) and is moving downward at the right wall (negative V at $x/L = 1$). These directions force the U component to be positive near the upper wall and to be negative near the lower wall, which initiate the clockwise rotation of the fluid inside the cavity. Another noticeable point is that the maximum value of the non-dimensional V is greater than that of the non-dimensional U value due to the effect of buoyant forces at the vertical walls.

The Variation of Nusselt Number

Results of the local Nusselt numbers Nu , Figure (6), show the effect of Ra on the variation of the local Nusselt number with the coordinate Y . The figure shows that the peaks of Nusselt numbers are located at the bottom of the hot wall and the top of the cold wall. The high velocity fluid at the bottom of the cold wall impinges to the bottom of the hot wall and causes this increase of the Nusselt number. Then the Nusselt number remains nearly constant in the middle between the hot and cold walls, before decreasing because of the separation of the fluid at the top of the hot wall and at the bottom of the cold wall. The maximum value of Nu increases with increasing Rayleigh number to enhance the effect of convection mode of heat transfer.

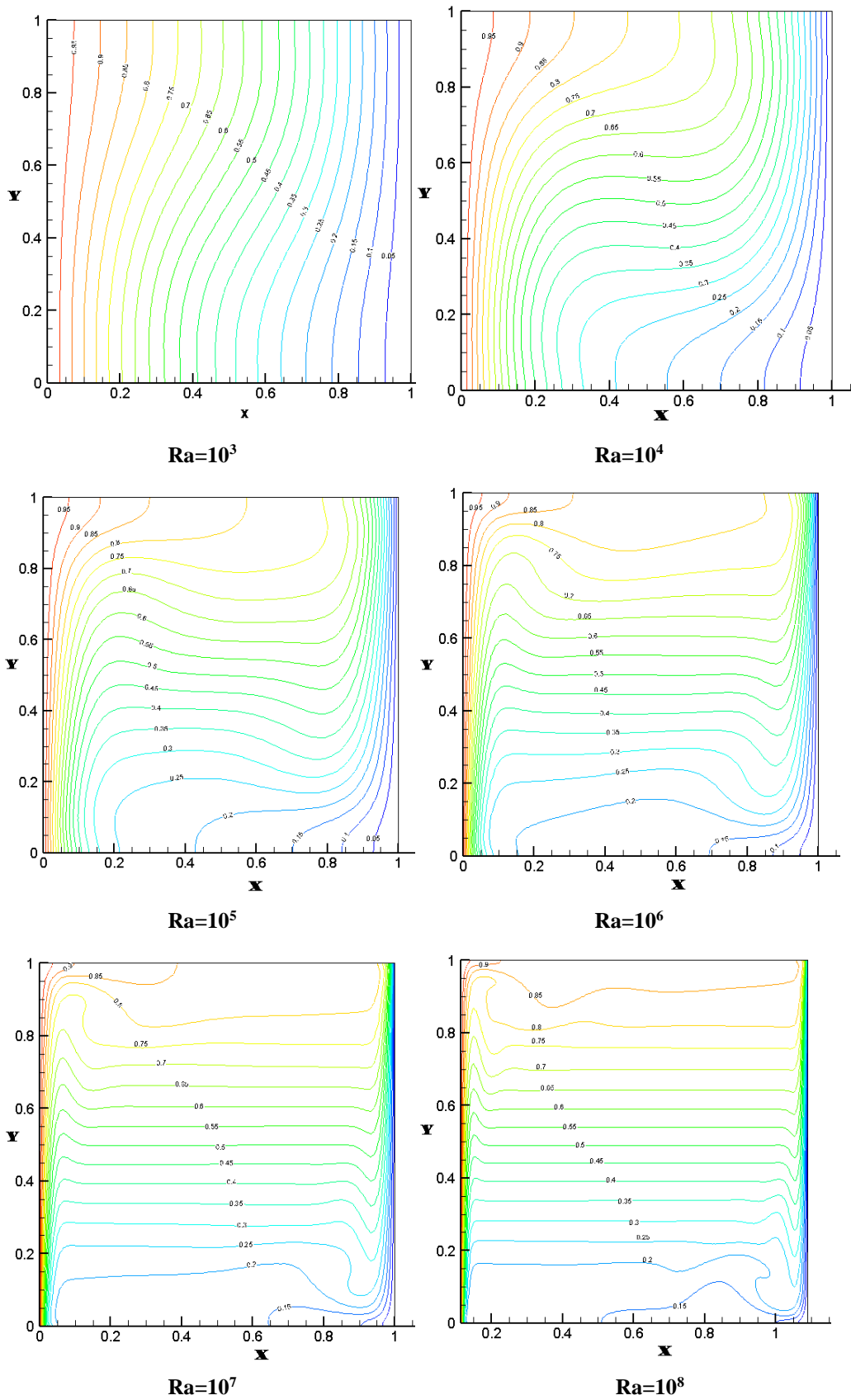


Figure 3: Contour plots of temperature θ for $Ra = 10^3 - 10^8$

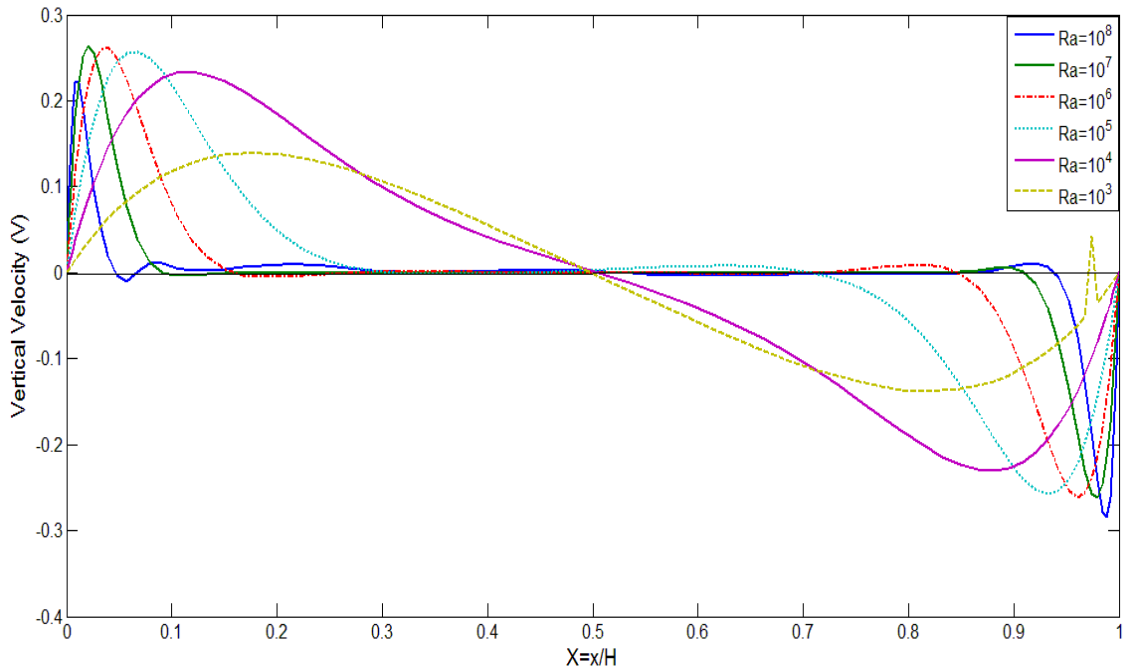


Figure 4: Non-dimensional vertical velocity component in the horizontal mid-plane

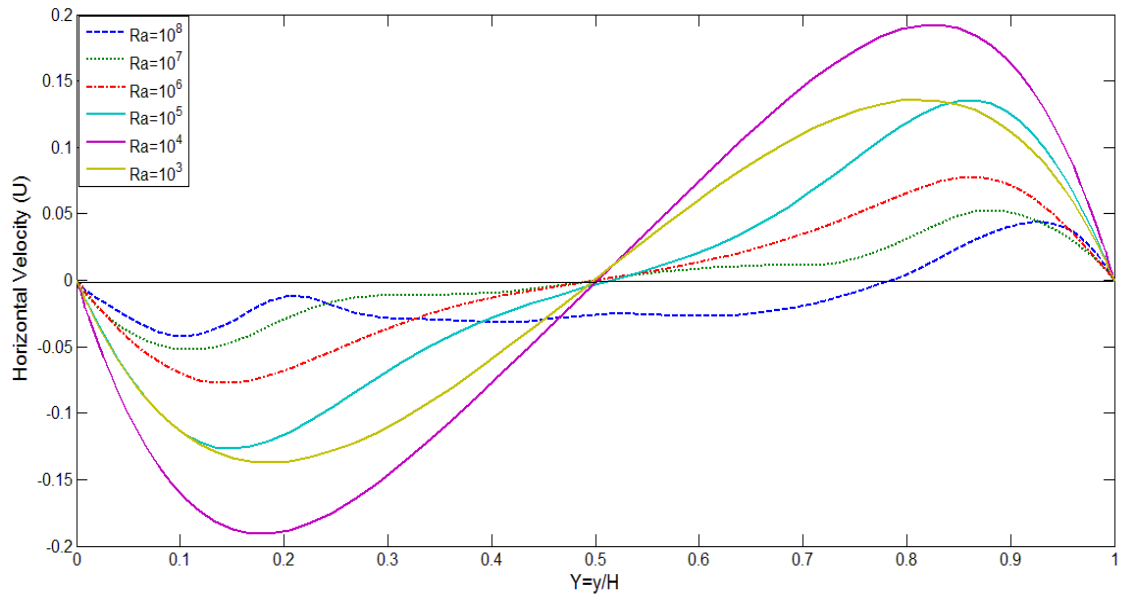


Figure 5: Non-dimensional horizontal velocity component in the vertical mid-plane

Correlation between the averages

Nusselt number and Rayleigh number

The results of the present calculation were fitted to the equation $\overline{Nu} = aRa^b$ and the values of a and b are compared with similar results by Markatos and Pericleous, Barakos y col and Henkes *et al* in Table (4). It is shown that there is good agreement between the results of this paper and the previous results.

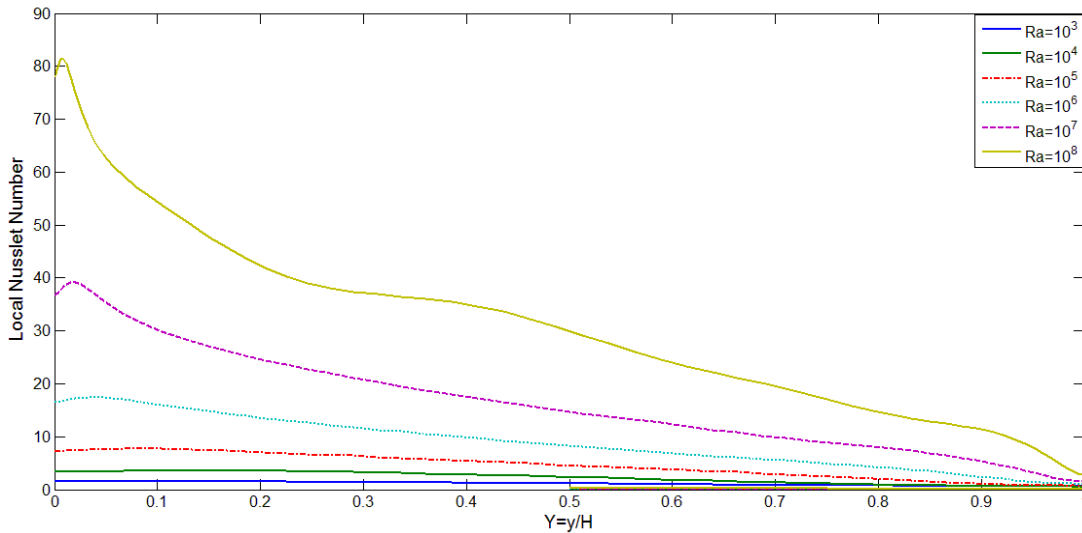


Figure 6: local Nusselt number with different Rayleigh numbers at hot wall

Table 4: Comparison of values a and b for correlation $Nu=a Ra^b$.

	a	b	Range
Present work	0.145	0.303	$10^3 < Ra < 10^6$
Barakos y col. (1994)	0.142	0.299	$10^3 < Ra < 10^6$
Markatos & Pericleou	0.143	0.299	$10^3 < Ra < 10^6$
Henkes et Al	0.304	0.25	
Present work	0.175	0.283	$10^6 < Ra < 10^8$

The relation between the average Nusselt number and the Rayleigh number using the results of this paper is found to be:

$$\overline{Nu} = 0.145 Ra^{0.303}$$

CONCLUSIONS

Overall conclusion

From the results of this research, it can be concluded that:

- A good agreement was found between the results of this present model and the Benchmark results of [3].
- A grid size of 80×80 produced an acceptable accuracy when compared with the benchmark results of [3].
- Power law scheme ran faster than both the upwind and central scheme.
- The average Nusselt number at the hot left side wall increased with increasing Rayleigh number.
- The local Nusselt number at the hot left side wall had a maximum value at the bottom.
- The results obtained for all parameters have an error of less than 1% compared with

benchmark numerical results of [3].

Scope for Further Study:

Since the Fortran code takes a long time (for high resolution and in turbulent regime simulation - next stage of the study) , we need more efficient methods to save and optimize computing resources (RAM and CPU time). The following aspects need to be investigated:

- Improving the Solver (use of e.g. Conjugated Gradient Method , Multigrid method, strongly implicit procedure, etc...).
- Improved SIMPLE-type procedures e.g.: SIMPLER, SIMPLEC, SIMPLEX, PISO, etc.,)
- Using of unstructured grid approach and code development for complicated geometries.
- The use of higher Order Differencing Schemes(QUICK Scheme, TVD.....etc.).

REFERENCES

- [1] Batchelor, G. K. "Heat Transfer by Free Convection across a Closed Cavity between Vertical Boundaries at Different Temperatures", Appl. Maths, Vol. 12, pp.209-233. 1954.
- [2] J. O. Wilkes and S. W. Churchill "The finite-difference Computation of Natural Convection in a Rectangular Enclosure". American Institute of Chemical Engineers Journal, 12(1):161–166, 1966.
- [3] G. de Vahl Davis. "Natural Convection of Air in a Square Cavity, a Benchmark Numerical Solution". Int. J. Numer. Meth. Fl., 3(3):249-264, (1983).
- [4] R. A. W. M. Henkes, "Natural Convection Boundary Layers", PhD Thesis, Technical University of Delft, the Netherlands, 1990.
- [5] R.A.W.M. Henkes, F.F. Van Der Vlugt, and C.J. Hoogendoorn. "Natural Convection Flow in a Square Cavity Calculated with Low Reynolds Number turbulence models". International Journal of Heat and Mass Transfer, 34(2):377–388, 1991.
- [6] Le Quere, P. Accurate solutions to the square thermally driven cavity at high Rayleigh number. Centre National de la Recherche Scientifique LIMSIS (Orsay, France), Notes et Documents 90-2. 1990.
- [7] G. Barakos, E. Mitsoulis, D. Assimacopoulos, "Natural Convection Flow in a Square Cavity Revisited: Laminar and Turbulent Models with Wall Functions, "Internat. J. Numer. Methods in Fluids 18 695–719 (1994).
- [8] N.C. Markatos, K.A. Pericleous, "Laminar and Turbulent Natural Convection in an Enclosed Cavity", Int. J. Heat Mass Transfer 27 (1984) 772–775.
- [9] T. Fusegi, J.M. Hyun, K. Kuwahara, B. Farouk, "A Numerical Study of Three-Dimensional Natural Convection in a Differentially Heated Cubical Enclosure", Int.J. Heat Mass Transfer 34 1543–1557 (1991) .
- [10] A. D’Orazio, M. Corcione , G. P. Celata, "Application to Natural Convection Enclosed Flows of a Lattice Boltzmann BGK Model Coupled with a General Purpose Thermal Boundary Condition", International Journal of Thermal Sciences 43 575–586.fgv (2004).
- [11] R. Puragliesi, A. Dehbi, E. Leriche, A. Soldati, and M. O. Deville, "DNS of Buoyancy-Driven Flows and Lagrangian Particle Tracking in a Square Cavity at High Rayleigh Numbers", Int. J. Heat Fluid Flow 32, 915 (2011).
- [12] Malalaseera W., and Versteeg H. K., "An Introduction to Computational Fluid Dynamics the Finite Volume Method", Pearson Education Limited, Harlow, England, 1995.
- [13] ANDERSON, J D, "Computational Fluid Dynamics". McGraw-Hill, New York, 1995.

- [14] J. Guet, M. Reggio, and P. Vasseur, "Natural Convection of Nano Fluids in a Square Enclosure with a Protruding Heater", *J. Heat Fluid Flow* 32, 915 (2012).
- [15] F. DURST: *An Introduction to The Theory of Fluid Flows*", Springer, Berlin, 2008.
- [16] <http://www.wikipedia.org>.

NOMENCLATURE

a	Coefficient of Discretization Equation (a_p, a_w, a_e, a_s, a_n)
cp	specific heat at constant pressure ($J\ kg^{-1}\ K^{-1}$)
D	concentration diffusion coefficient ($m^2\ s^{-1}$)
Gr	Grashof number
g	gravitational acceleration ($m\ s^{-2}$)
H	Cavity height
k	thermal conductivity ($W\ m^{-1}\ K^{-1}$)
Nu	Nusselt number
\overline{Nu}	Average Nusselt number
p	pressure (Pa)
P	dimensionless pressure
Ra	Rayleigh number
S	Source
T	temperature (K°)
u, v	velocity components ($m\ s^{-1}$)
U, V	dimensionless velocity components
x, y	x-, y-coordinates (m)
X, Y	dimensionless coordinates

Greek symbols

α	thermal diffusivity ($m^2\ s^{-1}$)
μ	dynamic viscosity ($kg\ m^{-1}\ s^{-1}$)
ν	kinematic viscosity ($m^2\ s^{-1}$)
ρ	density ($kg\ m^{-3}$)
β	thermal expansion coefficient (K^{-1})
θ	dimensionless temperature
ψ	dimensionless stream function
\tilde{O}	general scalar dependent variable
\tilde{A}	diffusion coefficient

Subscripts

H	high
L	low